ACS Catalysis

Research Article

pubs.acs.org/acscatalysis

Ag Alloyed Pd Single-Atom Catalysts for Efficient Selective Hydrogenation of Acetylene to Ethylene in Excess Ethylene

Guang Xian Pei,[†,‡,#] Xiao Yan Liu,[†,#] Aiqin Wang,[*,†] Adam F. Lee,[§] Mark A. Isaacs,[§] Lin Li,[†] Xiaoli Pan,[†] Xiaofeng Yang,[†] Xiaodong Wang,[†] Zhijun Tai,[§] Karen Wilson,[§] and Tao Zhang[*,†]

[†]State Key Laboratory of Catalysis, iChEM (Collaborative Innovation Center of Chemistry for Energy Materials), Dalian Institute of Chemical Physics, Chinese Academy of Sciences, Dalian 116023, China

[‡]University of Chinese Academy of Sciences, Beijing 100049, China

[§]European Bioenergy Research Institute, Aston University, Aston Triangle, Birmingham B4 7ET, United Kingdom

Supporting Information

ABSTRACT: Semihydrogenation of acetylene in an ethylene-rich stream is an industrially important process. Conventional supported monometallic Pd catalysts offer high acetylene conversion, but they suffer from very low selectivity to ethylene due to overhydrogenation and the formation of carbonaceous deposits. Herein, a series of Ag alloyed Pd single-atom catalysts, possessing only ppm levels of Pd, supported on silica gel were prepared by a simple incipient wetness coimpregnation method and applied to the selective hydrogenation of acetylene in an ethylene-rich stream under conditions close to the front-end employed by industry. High acetylene conversion and simultaneous selectivity to ethylene was attained over a wide temperature window, surpassing an analogous Au alloyed Pd single-atom system we previously reported. Restructuring of AgPd nanoparticles and electron transfer from Ag to Pd were evidenced by in situ FTIR and in situ XPS as a function of increasing reduction temperature. Microcalorimetry and XANES measurements support both geometric and electronic synergetic effects between the alloyed Pd and Ag. Kinetic studies provide valuable insight into the nature of the active sites within these $AgPd/SiO_2$ catalysts, and hence, they provide evidence for the key factors underpinning the excellent performance of these bimetallic catalysts toward the selective hydrogenation of acetylene under ethylene-rich conditions while minimizing precious metal usage.

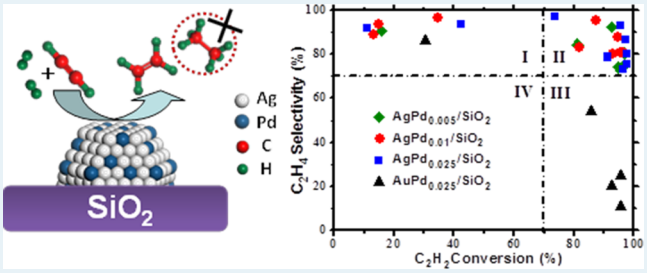

KEYWORDS: *acetylene hydrogenation, excess ethylene, silver, Pd single-atom, FTIR, in situ XPS, microcalorimetry*

1. INTRODUCTION

Ethylene is one of the most important industrial products of the petrochemical industry, principally used for polyethylene production, and predominantly produced by the pyrolysis of hydrocarbons, such as the thermal cracking of naphtha. Small amounts of coproduced acetylene (~1%) are poisonous to the downstream catalysts employed for subsequent ethylene polymerization and must therefore be first diminished to an acceptable level.[1,2] The preferred method for removing acetylene from an ethylene stream is its catalytic partial hydrogenation to additional ethylene. This is completed via so-called front-end and/or tail-end configurations.[3,4] In the front-end process, hydrogenation occurs with excess hydrogen in the feed gas, often resulting in overhydrogenation of acetylene to ethane and other byproducts. In tail-end hydrogenation, the ethylene feed gas is further purified to remove methane and other light hydrocarbons prior to the addition of a controlled amount of hydrogen to minimize overhydrogenation of acetylene to ethane. Supported Pd catalysts are commonly used in both of these processes. Unfortunately, although acetylene conversions are usually high, significant quantities of ethylene in the feedstock are also overhydrogenated to ethane, lowering the atom economy.[5−8] Furthermore, carbonaceous deposits formed on the catalyst surface can encapsulate active Pd sites causing significant on-stream deactivation.[9,10]

Low coordination Pd atoms in the surface of supported Pd nanoparticles have been generally regarded as the most active sites for acetylene hydrogenation, but are also recognized as responsible for low selectivity to ethylene due to strong reactant and product adsorption on contiguous Pd sites.[11,12] A common approach to improve ethylene selectivity over supported Pd nanocatalysts is to block some of these active sites by modification with a second metal (e.g., Au,[13] Ag,[14,15] Cu[16]), metal oxide (e.g., La_2O_3,[17] TiO_2[18]), or inert material (e.g., porous silica[19] or carbonaceous deposits formed by pretreatment with feed gases[20]). Although such modified catalysts exhibit superior selectivity to ethylene, this approach sacrifices a high concentration of expensive Pd sites. In addition, large amounts

Received: April 2, 2015
Revised: May 3, 2015
Published: May 5, 2015

DOI: 10.1021/acscatal.5b00700
ACS Catal. 2015, 5, 3717−3725

of ethylene in the feedstock still undergo overhydrogenation to ethane at higher reaction temperatures, especially in front-end hydrogenation wherein high hydrogen concentrations are present. The development of a high-activity Pd catalyst for acetylene hydrogenation, which also exhibits high selectivity to ethylene and efficient precious palladium metal usage, remains a challenge.

Downsizing conventional noble metal nanoparticles to single atoms affords one route to enhance the atomic efficiency of supported noble metal catalysts. Literature methods often anchor single atoms at defects on reducible oxide supports,[21−23] dispersed across the surface of graphene,[24] or inserted into zeolite frameworks.[25] An alternative approach is through alloying with a second metal.[26,27] Through alloying Au atoms within Pd clusters, Zhang et al. constructed a "Crown-Jewel" structured catalyst with single Au atoms alloyed atop Pd clusters that showed excellent activity for H_2O_2 decomposition.[28] Utilizing physical vapor deposition, Sykes's and co-workers alloyed single Pd atoms into Cu (111) surfaces, discovering that these isolated Pd atoms were able to activate molecular H_2, rendering the alloy surfaces much more efficient for the selective hydrogenation of styrene and acetylene than corresponding monometallic Pd and Cu systems.[29,30]

Previously, we synthesized Au alloyed Pd single-atom catalyst supported on silica gel by a two-step method and found that these offered far superior selectivity to ethylene under front-end conditions than an analogous monometallic Pd catalyst.[31] However, the high cost of Au and complexity of the preparation method renders this methodology uneconomic for industrial applications. It is therefore desirable to find a lower cost and more efficient partner metal with which to develop alloyed Pd single-atom catalysts. Herein, Ag was chosen as a substitute to prepare alloyed Pd single-atoms via a simple incipient wetness coimpregnation method. Surprisingly, the Ag alloyed Pd single-atom catalyst exhibited both higher acetylene conversion and selectivity to ethylene with time on stream than our previous Au alloyed Pd single-atom counterpart at similar Pd loadings. Furthermore, the selectivity to ethylene increased with increasing reduction temperature over $AgPd/SiO_2$. The structural evolution of this new Ag alloyed Pd single-atom catalyst was investigated through XRD, HAADF-STEM, in situ XPS, XAS, in situ FT-IR and microcalorimetry of ethylene adsorption.

2. EXPERIMENTAL SECTION

2.1. Catalyst Preparation. A range of catalysts with different Pd/Ag atomic ratios were prepared by incipient wetness coimpregnation. First, silica gel (Qingdao Ocean Chemical Plant with a Brunauer−Emmett−Teller (BET) surface area of 463 $m^2 \cdot g^{-1}$) was impregnated with a mixture of $Pd(NO_3)_2$ and $AgNO_3$ solutions to achieve a nominal Ag loading of 5 wt % and different Pd/Ag atomic ratios. Samples were subsequently dried at 80 °C for 10 h prior to calcination in air at 400 °C for 2 h. The as-prepared catalysts are denoted $AgPd_x/SiO_2$, with x denoting the Pd/Ag atomic ratio.

2.2. Catalyst Characterization. Actual metal loadings of the as-prepared catalysts were quantified by inductively coupled plasma spectrometry (ICP-AES) on a Thermo IRIS Intrepid II XSP instrument with results shown in Table 1.

XRD patterns were collected on a PW3040/60 X' Pert Pro Super (PANalytical) diffractometer, operating at 40 kV and 40 mA using a Cu Kα radiation source (λ = 0.15432 nm) with a scanning angle (2θ) of 10−80°.

High-angle annular dark-field scanning transmission electron microscopy (HAADF-STEM) images were collected on a JEM-2100F instrument equipped with STEM dark-field (DF) detector operating at 200 kV. Prior to measurement, a small amount of the reduced (at 250 or 500 °C) catalysts was ultrasonically dispersed by ethanol, and several drops of the resulting suspension placed on copper microgrid covered with carbon polymer and dried at room temperature. Particle size distributions of as-prepared catalysts were obtained by measuring more than 200 particles from different areas.

Temperature-programmed reduction (TPR) experiments were performed on a Micromeritics AutoChem II 2920 automated characterization system. First, approximately 200 mg of the calcined sample was loaded into a U-shaped quartz tube and pretreated with Ar for 10 min, the gas flow was then switched to 10 vol % H_2/Ar, and the catalyst was heated to 500 °C at 10 °C·min^{-1}.

In situ X-ray photoelectron spectroscopy (XPS) was undertaken using a Kratos AXIS HSi spectrometer equipped with a charge neutralizer and magnetic focusing lens employing a monochromated Al X-ray source (1486.7 eV).[32] Samples were reduced in situ at different temperatures for 0.5 h in the analyzer chamber under H_2 pressures of up to 2×10^{-7} Torr. Spectra were subsequently collected at normal emission using an analyzer pass energy of 40 eV at room temperature. Spectra were energy referenced to the valence band and Si 2p peak at 103.4 eV binding energy (BE).

X-ray absorption near-edge structure (XANES) spectra at Pd K-edge were obtained at the BL14W1 at Shanghai Synchrotron Radiation Facility (SSRF), Shanghai Institute of Applied Physics (SINAP), China. A double Si(311) crystal monochromator was used for energy selection with a Pd foil employed for energy calibration. Prior to experiments, samples were reduced at 400 °C for 1 h, purged under He at the same temperature for 10 min, and subsequently cooled to room temperature and evacuated before transferred to a glovebox and sealed in Kapton without exposure to air. Fluorescence Pd K-edge spectra were collected at room temperature with a solid state detector.

Fourier-Transform Infrared Spectra (FTIR) were collected on a Bruker EQUINOX 55 infrared spectrometer with a DTGS detector. Prior to CO chemisorption, as-prepared samples were pretreated at 250 or 500 °C under flowing 80 vol % H_2/He (20 mL·min^{-1}) for 1 h, followed by evacuation at the same temperature for 0.5 h, then cooled to room temperature. After pretreatment, a background spectrum was collected from samples and subtracted automatically from subsequent spectra. CO adsorption experiments were carried out sequentially on a single sample. Gas-phase CO spectra were collected at the same pressure and subtracted from the corresponding sample spectra. CO was purified with a liquid nitrogen trap.

Microcalorimetric measurements of ethylene adsorption were performed at 40 °C with a BT 2.15 heat-flux calorimeter connected to a gas handling system and a volumetric system equipped with MKS 698A baratron capacitance manometers to give precise pressure measurement ($\pm 1.33 \times 10^{-2}$ Pa).[33] Prior to measurement, samples were pretreated at different temperatures under flowing H_2 for 1 h, evacuated for 0.5 h at the same temperature to remove adsorbed H_2, cooled to room temperature in vacuo, and subsequently isolated by refilling with He and sealing in a thin quartz tube. These sealed quartz tubes were placed into the calorimetric cell immersed within the isothermal calorimetric block.

DOI: 10.1021/acscatal.5b00700
ACS Catal. 2015, 5, 3717−3725

2.3. Catalyst Evaluation. The partial hydrogenation of acetylene in excess ethylene was carried out in a quartz reactor. Prior to the activity tests, 30 mg of catalysts were pretreated under flowing 80 vol % H_2/He (20 mL·min^{-1}) at different temperatures for 1 h and purged with He (20 mL·min^{-1}) at the same temperature. After cooling to room temperature, a gas mixture approximating the front-end condition with 1.0 vol % C_2H_2, 20.0 vol % H_2 and 20.0 vol % C_2H_4 balanced with He was introduced into the reactor with a space velocity of 60,000 mL·h^{-1}·g^{-1}. The feed gas purities were as follows: H_2 (UHP, 99.999%), He (UHP, 99.999%), C_2H_2 and C_2H_4 (mixture of 4.77 vol % C_2H_2 in C_2H_4 with about 300 ppm of C_2H_6 impurity from Dalian Special Gases Co., Ltd.). All gas flows were controlled by mass flow controllers. The reaction temperature was held constant for 25 min prior to ramping to the next temperature point. The gas composition from the microreactor outlet was analyzed by online gas chromatography (Agilent Technologies 6890N) equipped with a FID detector.

In accordance with our former study,[31,34−36] C_2H_4 and C_2H_6 were the only C2 products detected by GC. Negligible oligomers were formed during the hydrogenation process due to the short contact time. Acetylene conversion and selectivity to ethylene were calculated as follows:

$$\text{Conversion} = \frac{C_2H_2(\text{feed}) - C_2H_2}{C_2H_2(\text{feed})} \times 100\% \quad (1)$$

$$\text{Selectivity} = \left(1 - \frac{C_2H_6 - C_2H_6(\text{feed})}{C_2H_2(\text{feed}) - C_2H_2}\right) \times 100\% \quad (2)$$

Kinetic studies of acetylene hydrogenation were undertaken with the same reaction system. Both $AgPd_{0.01}/SiO_2$ and $Pd_{0.01}/SiO_2$ catalysts were reduced at 400 °C, at which the $AgPd_{0.01}/SiO_2$ showed the optimized catalytic performance. In order to maintain acetylene conversion <15%, gas flow rates were varied from 60 mL·min^{-1} to 180 mL·min^{-1}. H_2 reaction orders were calculated for concentrations between 14 vol % to 22 vol % while the C_2H_2 and C_2H_4 concentrations were held constant at 1 vol % and 20 vol %, respectively. Activation energies were determined between 70 and 100 °C with feed gas compositions of 1 vol % C_2H_2, 20 vol % C_2H_4, and 20 vol % H_2 balanced with He.

3. RESULTS AND DISCUSSION

3.1. Selective Hydrogenation of Acetylene. The catalytic activity of the monometallic Ag/SiO_2 catalyst was first evaluated, showing negligible activity for all prereduction temperatures (Figure S1a). In contrast, the monometallic Pd/SiO_2 catalyst showed excellent activity, even at temperatures as low as 80 °C, but exhibited extremely poor selectivity to ethylene, strongly favoring ethane even at very low Pd loadings (akin to the bimetallic catalyst) following both 250 and 400 °C prereduction (Table 1 and Figure S1b). The addition of trace Pd to the Ag/SiO_2 catalyst dramatically enhanced the catalytic performance (Figure 1), with the resulting conversion/selectivity a strong function of Ag/Pd ratio and prereduction temperature. After 250 °C reduction, acetylene conversion over $AgPd_{0.025}/SiO_2$ reached 100% at 80 °C (Figure 1a); however, ethylene selectivity was ∼−200% (Figure 1b), consistent with the hydrogenation of significant ethylene in the feedstock to ethane. Furthermore, with increasing reaction temperature, this undesired loss of ethylene was even higher than that at 80 °C. However, surprisingly, the selective hydrogenation of acetylene to ethylene increased greatly with rising reduction temperature: following 400 °C prereduction, ethylene selectivity rose above 0 at 120 °C reaction temperature; after 500 °C prereduction, ∼80% selectivity to ethylene was achieved with high acetylene conversions of over 93% between 120 and 320 °C. This performance is superior to previous literature wherein both acetylene and large amounts of ethylene underwent hydrogenation to ethane at higher reaction temperatures (Table S1). Further increases in reduction temperature to 550 °C proved less beneficial, with acetylene conversion decreasing, albeit at the expense of ethylene selectivities reaching >90%.

Table 1. Elemental Analysis of As-Prepared $AgPd/SiO_2$ Catalysts

		nominal loading		actual loading[a]	
entry	catalysts	Ag/Pd (atomic ratio)	Pd (ppm)	Ag (wt %)	Pd (ppm)
1	Ag/SiO_2	--	--	5.08	--
2	$AgPd_{0.005}/SiO_2$	200	247	4.90	168
3	$AgPd_{0.01}/SiO_2$	100	493	4.86	463
4	$AgPd_{0.025}/SiO_2$	40	1233	4.76	1016
5	$Pd_{0.01}/SiO_2$	--	493	--	426

[a]Determined by ICP-AES.

Similar qualitative behavior was observed with decreasing Pd content as a function of both reaction temperature (Figure 1c−f), with acetylene conversion decreasing slightly accompanied by a rise in ethylene selectivity as the prereduction temperature was increased. However, higher reaction temperatures were required for the $AgPd_{0.01}/SiO_2$ and $AgPd_{0.005}/SiO_2$ catalysts to attain comparable conversion to the higher loading $AgPd_{0.025}/SiO_2$, the former exhibited superior ethylene selectivity following lower temperature prereduction, with selectivities exceeding 80% after 400 and 300 °C prereduction, respectively. In other words, as the palladium loading increases, higher prereduction temperatures are necessary to achieve what seems likely a common optimal structure/active site density. Compared with our previous Au alloyed Pd single-atom catalysts, the selectivity toward ethylene was improved greatly, possibly reflecting superior isolation of atomically dispersed Pd with the surface of silver nanoparticles (geometry) and/or different charge transfer between Ag and Pd (electronic), as discussed in Sections 3.2 and 3.3.

The optimal results for the $AgPd/SiO_2$ catalysts from Figure 1 ($AgPd_{0.025}/SiO_2$, $AgPd_{0.01}/SiO_2$, and $AgPd_{0.005}/SiO_2$ catalysts reduced at 500, 400, and 300 °C, respectively) and the $AuPd_{0.025}/SiO_2$ catalyst reported previously[31] are summarized in Figure 2. Values for the $AuPd_{0.025}/SiO_2$ catalyst lie in Region III wherein selectivity to ethylene was relatively poor, although acetylene conversion was high. In contrast, the majority of values for the $AgPd/SiO_2$ catalysts in this work fall into Region II wherein high conversion and selectivity are achievable concurrently. Even Pd loadings as low as 168 ppm (the $AgPd_{0.005}/SiO_2$ catalyst) are sufficient to deliver 92.6% conversion of acetylene with 92.3% selectivity of ethylene (Figure 2, green diamond point in top-right corner of Region II.), that is, an 85.5% yield, representing the best performance reported to date (Table S1). In literature reports, high acetylene conversion was accompanied by significantly lower selectivity than our present work, irrespective of reaction temperature: the lower reaction temperatures of entries S1−S5 were associated with poorer performance in terms of conversion and/or selectivity; the high activity (>90% conversion) reported in entries S6−S7 at higher reaction temperatures than our work offered significantly poorer selectivity. Furthermore, the Pd loading in our catalyst is much

DOI: 10.1021/acscatal.5b00700
ACS Catal. 2015, 5, 3717−3725

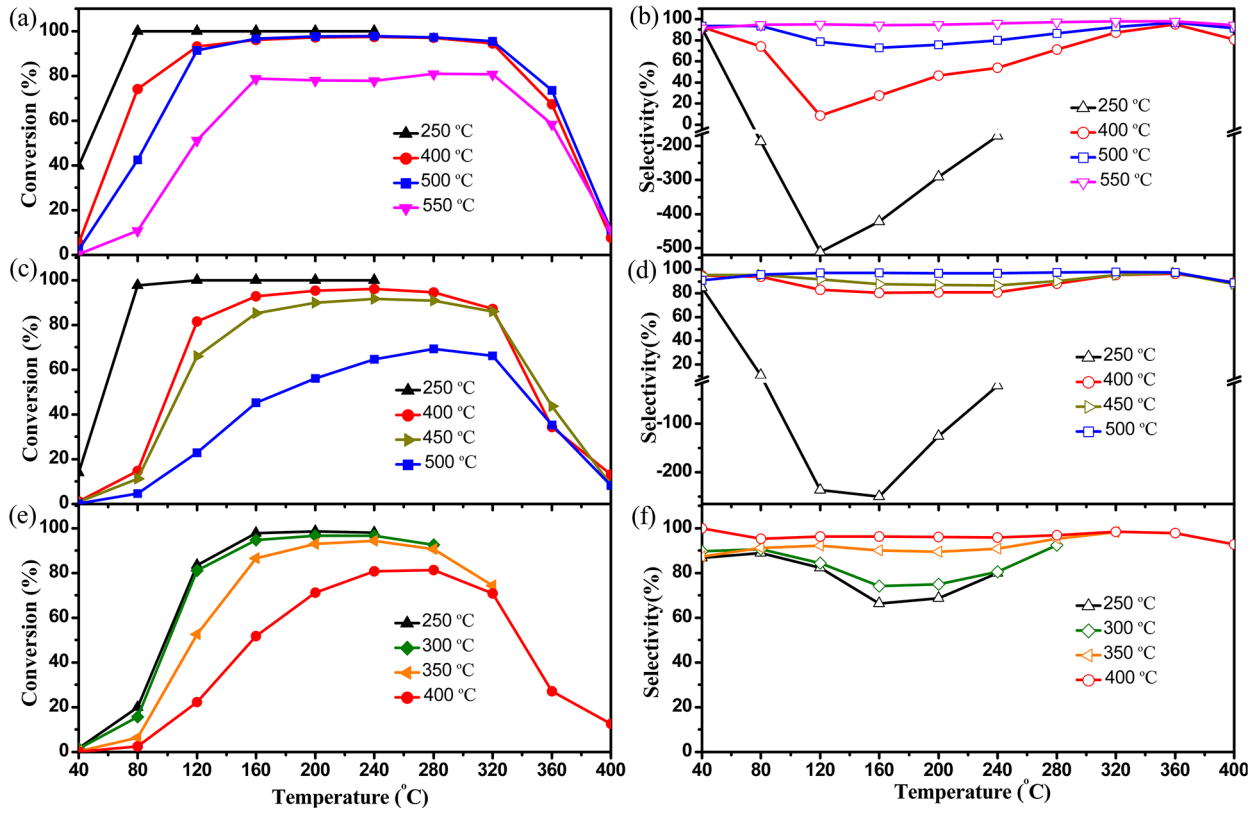

Figure 1. (a, c, e) Acetylene conversion and (b, d, f) ethylene selectivity as a function of reaction temperature over (a, b) $AgPd_{0.025}/SiO_2$, (c, d) $AgPd_{0.01}/SiO_2$ and (e, f) $AgPd_{0.005}/SiO_2$ catalysts at different prereduction temperatures.

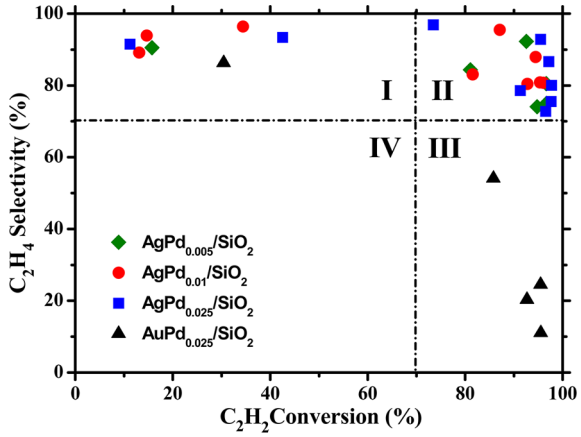

Figure 2. Optimal ethylene selectivity versus acetylene conversion over $AuPd_{0.025}/SiO_2$ and $AgPd/SiO_2$ bimetallic catalysts.

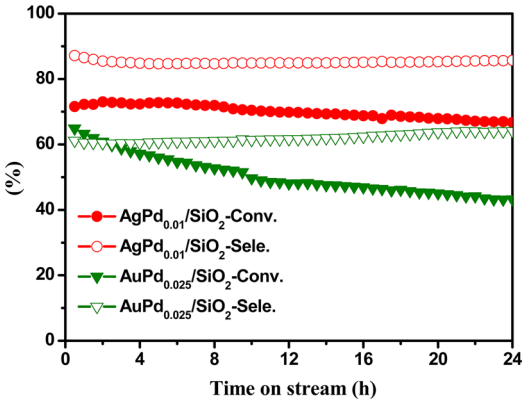

Figure 3. Ethylene selectivity (hollow) and acetylene conversion (solid) with time on stream for selective hydrogenation of acetylene to ethylene at 160 °C over $AgPd_{0.01}/SiO_2$ and $AuPd_{0.025}/SiO_2$ catalysts, reduced at different temperatures.

lower than literature materials (Table S1, entries S1−S7), offering outstanding Pd atom efficiency.

Catalyst durability is of paramount importance for the industrial selective hydrogenation of acetylene. Hence, the long-term stability of a $AgPd_{0.01}/SiO_2$ catalyst subject to the optimal 400 °C prereduction was explored, under more challenging reaction conditions of higher space velocity (240 000 $mL{\cdot}h^{-1}{\cdot}g^{-1}$) at 160 °C. Figure 3 shows that the $AgPd_{0.01}/SiO_2$ catalyst outperforms our previously reported $AuPd_{0.025}/SiO_2$ catalyst possessing a similar Pd content in terms of both conversion and selectivity. Furthermore, acetylene conversion and ethylene selectivity remained almost unchanged over 24 h on-stream for $AgPd_{0.01}/SiO_2$, whereas acetylene conversion fell by 22% over this period for the $AuPd_{0.025}/SiO_2$ catalyst. This finding suggests that silver-rich $AgPd/SiO_2$ catalysts with optimized pretreatments and operating conditions are good potential candidates for commercialization.

3.2. Catalyst Characterization. It is clear that catalyst prereduction is critical to achieving an outstanding hydrogenation performance, and hence, the effect of pretreatment upon the structural and electronic properties of $AgPd/SiO_2$ catalysts was investigated.

3.2.1. Particle Size and Crystallinity. $AgPd_{0.025}/SiO_2$ and Ag/SiO_2 catalysts were first examined in order to assess the impact of Pd addition upon the nanoparticle. Powder XRD was performed as a function of pretreatment temperature (Figure 4). After 400

DOI: 10.1021/acscatal.5b00700
ACS Catal. 2015, 5, 3717−3725

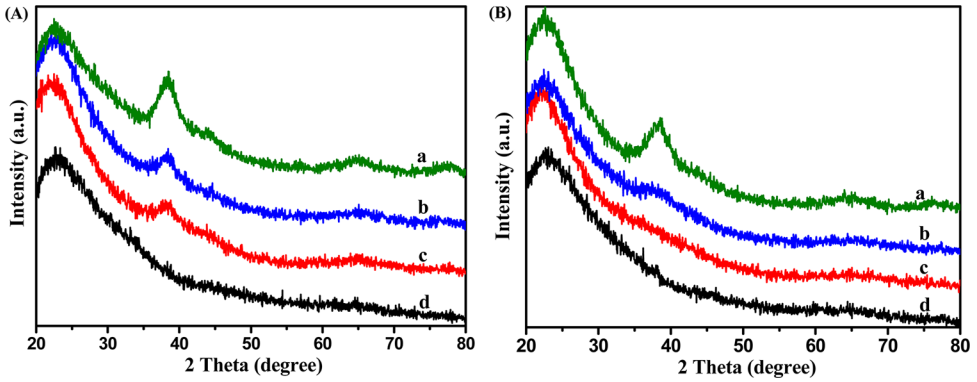

Figure 4. XRD patterns of (A) $AgPd_{0.025}/SiO_2$ and (B) Ag/SiO_2 catalysts as a function of pretreatment temperature: (a) 500 °C, (b) 400 °C, (c) 250 °C reduction, and (d) 400 °C calcination.

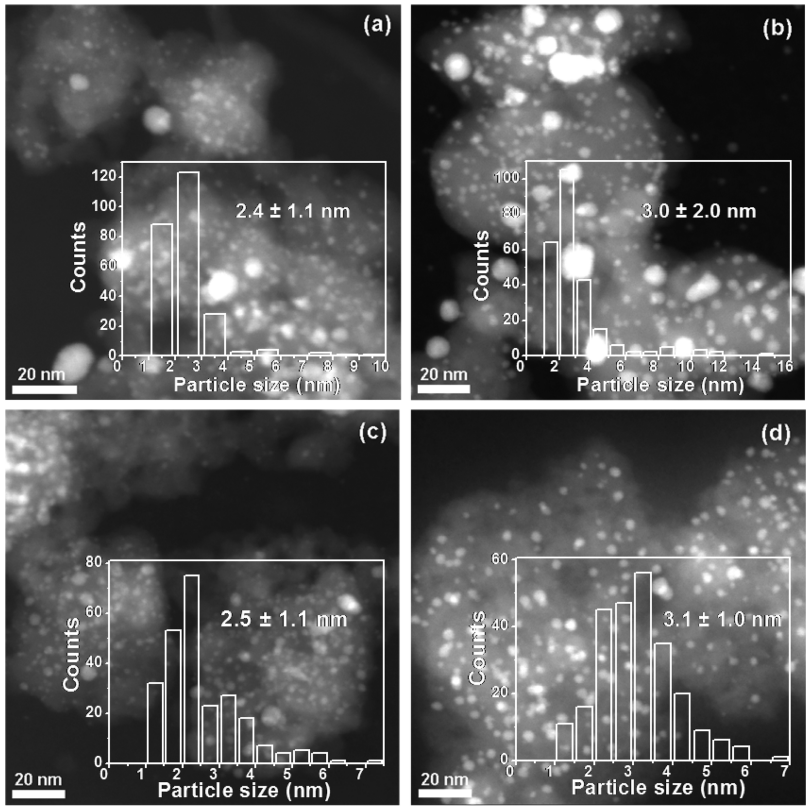

Figure 5. HAADF-STEM images of (a, b) Ag/SiO_2 and (c, d) $AgPd_{0.025}/SiO_2$ prereduced at 250 °C (a, c) and 500 °C (b, d).

°C calcination in air for 2 h, neither $AgPd_{0.025}/SiO_2$ nor Ag/SiO_2 exhibited reflections, indicating the presence of highly dispersed (<2 nm) particles and that calcination did not induce particle sintering. TPR measurements (Figure S2) revealed peaks characteristic of hydrogen consumption, confirming the presence of partially oxidized Ag and/or Pd following sample calcination at 400 °C and thermal decomposition of the nitrate precursors. As previously reported, such Ag oxide species could passivate the nanoparticle surfaces, enhancing their thermal stability[37] and necessitating the catalyst prereduction treatment employed. In contrast, prereduction resulted in the progressive evolution of diffraction features associated with face-centered cubic (fcc) Ag metal,[38] whose intensity increasing with reduction temperature corresponding to an increase in Ag nanoparticle size. In comparison with the monometallic Ag/SiO_2, the silver reflections were more pronounced for the $AgPd_{0.025}/SiO_2$ bimetallic catalyst; however, no reflections attributable to any Pd phase were detectable within the $AgPd_{0.025}/SiO_2$ catalyst, consistent with its low loading and likely highly dispersed nature.

Particle size differences between the Ag/SiO_2 and $AgPd_{0.025}/SiO_2$ catalysts were subsequently probed by HAADF-STEM. The particle sizes of both catalysts were similar between the as-calcined catalysts (Figure S3). Statistical comparison of particle size distributions also revealed little difference following their prereduction at 250 °C (Figure 5a,c), except for the presence of some larger (~10 nm) nanoparticles within the Ag/SiO_2 catalyst. Although the mean particle diameters of nanoparticles within both catalysts prereduced at 500 °C were also similar and slightly larger at 3 nm (Figure 5b,d), those within the $AgPd_{0.025}/SiO_2$ catalyst were more uniformly dispersed across the silica support than the monometallic Ag/SiO_2 catalyst. Silver-containing nanoparticles were thus sensitive to sintering with increasing

DOI: 10.1021/acscatal.5b00700
ACS Catal. 2015, 5, 3717−3725

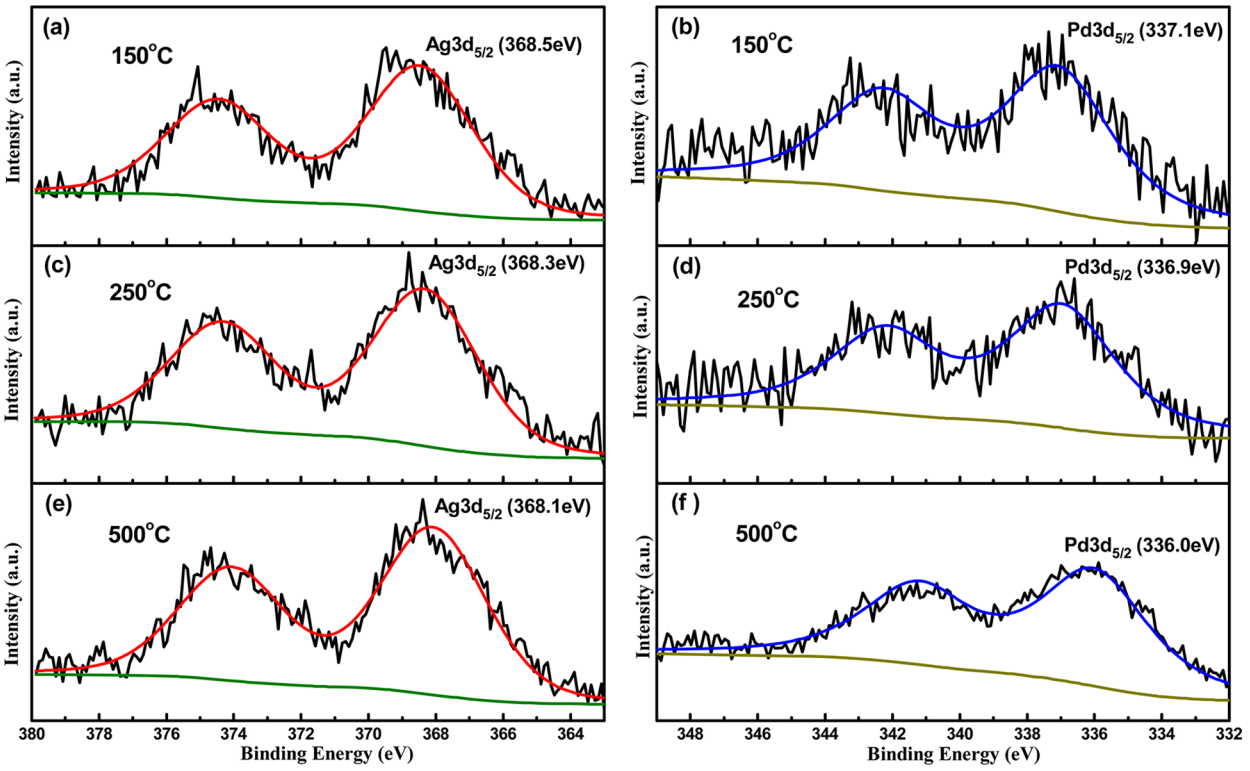

Figure 6. (a, c, e) Ag 3d and (b, d, f) Pd 3d XP spectra of Ag_1Pd_1/SiO_2 catalyst reduced in situ at 150 °C, 250 °C, 500 °C.

reduction temperature, in accordance with the reported thermal reducibility of Ag.[39] However, there is little correlation between particle growth and the substantial concomitant increase in ethylene selectivity seen in Figure 1b, or acetylene conversion (note the catalytic contribution from Ag/SiO_2 shown in Figure S1 is negligible).

3.2.2. Electronic Interactions between Ag and Pd. The electronic properties of surface Ag and Pd were investigated by in situ XPS, however due to the sensitivity limits of laboratory XPS instruments, for these studies the Pd loading was increased to 5 wt % through an identical preparation protocol. Figure 6 and Table S2 revealed that increasing the prereduction temperature from 150 to 500 °C decreased both Ag and Pd $3d_{5/2}$ BEs by 0.4 and 1.1 eV, respectively. TPR of the lower Pd loading bimetallic $AgPd/SiO_2$ catalysts (Figure S2) revealed only a single reduction peak around 90 °C, independent of Ag:Pd atomic ratio, indicating that these catalysts were likewise reduced at temperatures above 150 °C. Silver is unusual in exhibiting a decreased BE in its low valence state relative to the metal,[40,41] and hence the Ag 3d shift to lower BE is indicative of electron transfer to more electronegative Pd atoms present within a AgPd alloy phase. This hypothesis is consistent with the concomitant decrease in Pd 3d BE observed with reduction temperature, as expected for the formation of electron-rich (anionic) palladium. The increase in charge transfer with reduction temperature likely reflects the parallel decrease in Pd/Ag surface ratio, which implies a higher mean coordination number of silver atoms surrounding each Pd atom as the latter diffuses into the bulk of the bimetal nanoparticles.

In an effort to confirm the existence of charge transfer between Ag and Pd (and hence alloy formation), Pd K-edge XANES spectra of $AgPd_{0.01}/SiO_2$ and $Pd_{0.01}/SiO_2$ catalysts were measured (Figure 7). Palladium within both $AgPd_{0.01}/SiO_2$ and $Pd_{0.01}/SiO_2$ catalysts was fully reduced at 400 °C. However, the

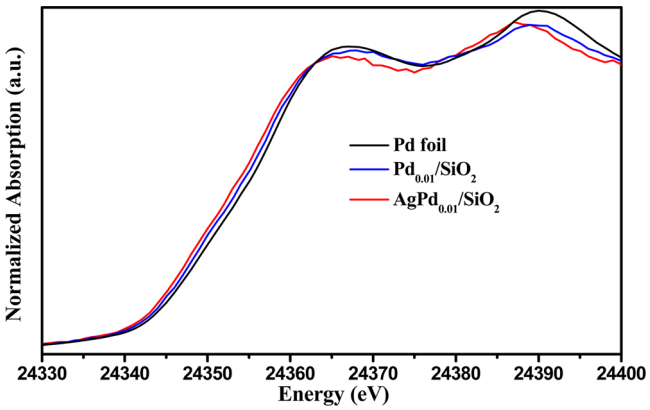

Figure 7. Normalized Pd K-edge XANES spectra of $Pd_{0.01}/SiO_2$ and $AgPd_{0.01}/SiO_2$ after 400 °C prereduction. A Pd foil reference spectrum is shown for comparison.

$AgPd_{0.01}/SiO_2$ white line was of lower intensity and shifted to lower energy relative to the monometallic counterpart and a Pd foil reference, consistent with a lower oxidation charge (i.e., anionic palladium, and hence charge transfer from silver to Pd)[8,41] and in accordance with the preceding XPS observations for the higher Pd loading Ag_1Pd_1/SiO_2 catalyst. It is highly probable that such charge transfer contributes to concomitant enhancement in ethylene selectivity with prereduction temperature.[18,42,43] Note that in our Au alloyed Pd single-atom system reported previously, the high electrongegativity of Au prohibits electron donation to Pd; this might account for the poorer catalytic performance of $AuPd/SiO_2$ versus $AgPd/SiO_2$ catalysts.

3.2.3. Evidence for Single Atom Pd Alloys. As a result of the extremely low Pd content of our bimetallic $AgPd/SiO_2$ catalysts, XRD, HAADF-STEM, and XPS were unable to provide insight into the local Pd structural/chemical environment. The

DOI: 10.1021/acscatal.5b00700
ACS Catal. 2015, 5, 3717−3725

distribution of Pd species in the catalyst surface was therefore probed by FTIR via CO chemisorption. Exposure of the $AgPd_{0.025}/SiO_2$ catalyst reduced at either 250 or 500 °C to 10 Torr CO and subsequent evacuated resulted in bands centered at 2165 and 2041 cm^{-1}, which we attribute to CO adsorbed on cationic Ag^{X+} species[39] and linearly adsorbed on Pd (Figure 8a).[44,45] The absence of any bridged-bound CO on the surface of

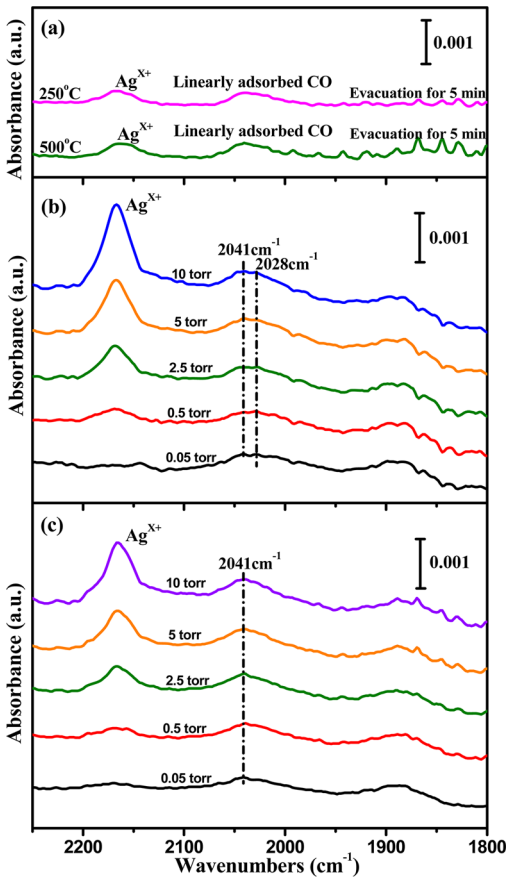

Figure 8. FTIR spectra of CO adsorbed over (a) $AgPd_{0.025}/SiO_2$ catalyst reduced at 250 or 500 °C; in situ FTIR spectra for $AgPd_{0.025}/SiO_2$ catalyst reduced at (b) 250 °C and (c) 500 °C as a function of CO pressure (after subtraction of gas-phase CO spectra).

the $AgPd_{0.025}/SiO_2$ catalysts reduced at 250 °C and 500 °C is strong evidence that the surface solely possesses single Pd atoms able to linearly bind CO, without any ensembles of neighboring Pd atoms. In conjunction with the preceding XANES measurements evidencing a Ag−Pd interaction, these FTIR observations are entirely consistent with the formation of Ag alloyed Pd single-atom structure.

Further insight into the nature of these isolated Pd sites within a Ag alloy in the $AgPd_{0.025}/SiO_2$ catalyst was obtained through in situ measurements under a constant CO background pressure. Figure 8b shows the resulting spectra (gas-phase CO contributions subtracted) for the $AgPd_{0.025}/SiO_2$ catalyst reduced at 250 °C, which show vibrational bands at 2028 and 2041 cm^{-1}, which can be reasonably ascribed to CO linearly adsorbed on single Pd atoms within facets and low coordination edge/corner sites of the nanoparticle surface, respectively.[46] As the CO pressure increased, the band at 2041 cm^{-1} increased in intensity relative to the 2028 cm^{-1} band, suggesting initial population of Pd atoms within terrace sites followed by subsequent edge/corner Pd atom adsorption. After higher-temperature reduction (Figure 8c), only a symmetric band at 2041 cm^{-1} was observed, independent of CO pressure, corresponding to low coordination Pd atoms, suggesting higher temperature reduction results in the loss of terrace Pd, possibly due to preferential silver surface segregation due to the latter's lower surface energy,[47] supported by a decrease in the Pd/Ag surface composition from XPS (Table S2).

3.3. Microcalorimetric Study of Selective Hydrogenation Active Sites. Microcalorimetry was employed to provide additional information on both the distribution and number of active surface sites as a function of ethylene probe molecule coverage. The initial heats of C_2H_4 adsorption over the $AgPd_{0.025}/SiO_2$ catalyst prereduced at 250, 400, and 500 °C was 96, 77, and 62 $kJ \cdot mol^{-1}$, respectively (Figure 9a); that is, the

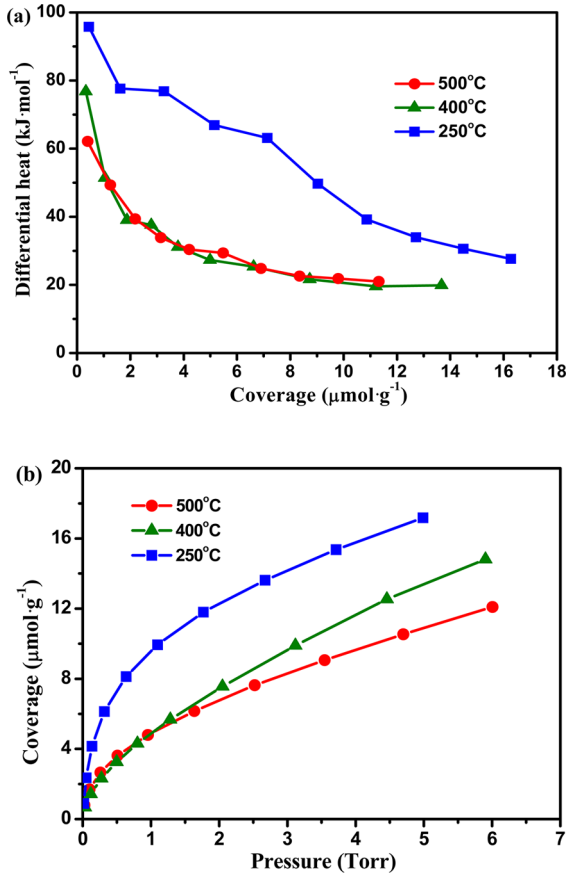

Figure 9. Differential heat of adsorption (a) and surface coverage (b) of C_2H_4 over $AgPd_{0.025}/SiO_2$ as a function of prereduction temperature.

initial C_2H_4 adsorption strength decreased with increasing reduction temperature, which resulted from the effect of Ag on Pd both geometrically and electronically, as the adsorption of C_2H_4 on Ag/SiO_2 is negligible.[48] This finding is expected to translate to an enhanced desorption rate of reactively formed ethylene from the surface of $AgPd/SiO_2$ catalysts prereduced at higher temperatures and would account for the observed increase in ethylene selectivity seen in Figure 1b.[4,49] Figure 9b shows the corresponding pressure-dependent surface coverage of C_2H_4 as a function of prereduction, which reveals a general decrease in the amount of C_2H_4 adsorbed over $AgPd_{0.025}/SiO_2$ with increasing reduction temperature from 9.0 $\mu mol \cdot g^{-1}$ (250 °C) to 4.5 $\mu mol \cdot g^{-1}$ (500 °C). These observations are in accordance with the particle sintering and silver surface segregation seen by XRD,

DOI: 10.1021/acscatal.5b00700
ACS Catal. 2015, 5, 3717−3725

XPS, and FTIR CO chemisorption, and related microcalorimetry measurements ,which have demonstrated that ethylene adsorption over Pd/SiO_2 is strongly suppressed by alloying with silver.[48]

Complementary ethylene microcalorimetry was performed over $AgPd_{0.025}/SiO_2$, $AgPd_{0.01}/SiO_2$, and $AgPd_{0.005}/SiO_2$ catalysts prereduced at 500, 400, and 300 °C, which correspond to the conditions necessary to achieve their respective optimum catalytic performance from Figure 1. The initial heats of C_2H_4 adsorption (~62−66 kJ·mol^{-1}) and surface coverage (4.5, 5.3, and 5.4 μmol·g^{-1}, respectively) over the three catalysts were almost the same (Figure S4), indicating the presence of chemically similar Pd surface sites, rationalizing their similar catalytic performance (Figures 1 and 2). It therefore appears that the exceptional activity and selectivity of our catalysts arise from unique Pd single atom sites distributed within a silver surface alloy, a matrix which modifies both the local structural and electronic environment of such isolated Pd centers to facilitate facile acetylene hydrogenation and subsequent rapid desorption of the resulting weakly bound ethylene product.

3.4. Selective Hydrogenation Kinetics. Additional kinetic analyses were undertaken to provide further insight into the catalytically active sites. Because H_2 activation plays a key role in the desired reaction, we first investigated the reaction order in H_2 over the $AgPd_{0.01}/SiO_2$ and corresponding monometallic $Pd_{0.01}/SiO_2$ catalysts, which possessed similar Pd loadings. As shown in Figure 10a, the H_2 reaction order over both catalysts were very similar at 1.11 versus 1.13, and close to literature values reported for monometallic Pd catalysts,[50,51] indicating that dissociative chemisorption of molecular H_2 occurred predominantly at Pd sites, with Ag a spectator in this step of the reaction pathway. This conclusion is in good agreement with the results of González et al, whose DFT calculations suggested that the H_2 activation was favored at Pd, rather than Ag, centers within AgPd bimetallic catalysts.[52]

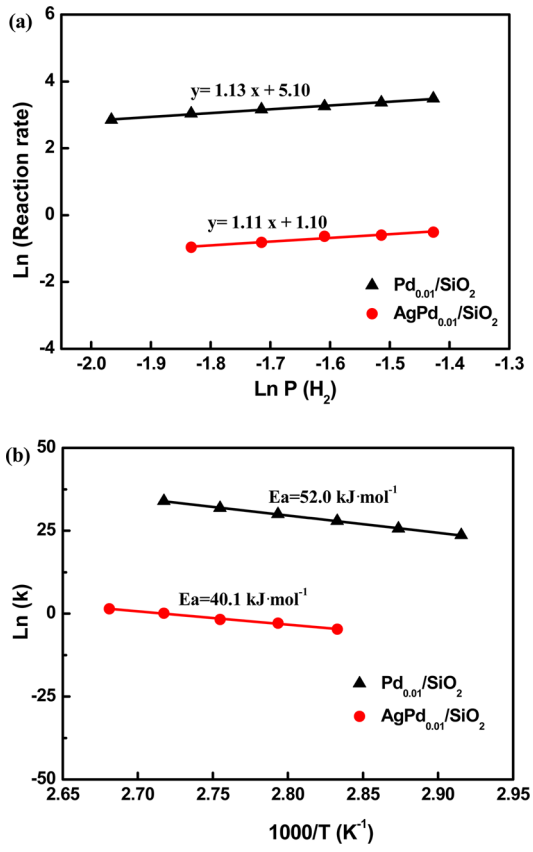

Figure 10. (a) H_2 pressure dependencies for $AgPd_{0.01}/SiO_2$ and $Pd_{0.01}/SiO_2$ catalysts at 80 °C, and (b) Arrhenius plots for C_2H_2 conversion over $Pd_{0.01}/SiO_2$ and $AgPd_{0.01}/SiO_2$ catalysts under a 1% C_2H_2, 20%H_2, 20% C_2H_4 gas mix balanced with He.

Apparent activation energies for C_2H_2 hydrogenation over the $Pd_{0.01}/SiO_2$ and $AgPd_{0.01}/SiO_2$ catalysts were 52.0 and 40.1 kJ·mol^{-1}, respectively (Figure 10b); that is, acetylene activation was approximately 12 kJ·mol^{-1} more facile over the Ag alloyed Pd single atom catalyst than the monometallic $Pd_{0.01}/SiO_2$ catalyst, which may account for the ability of the bimetallic single atom alloy catalyst to retain a high activity for acetylene conversion despite the extremely low concentration of surface Pd sites participating in the hydrogenation reactions.[4] Further investigations are necessary in order to elucidate whether this more facile C_2H_2 activation over the bimetallic $AgPd/SiO_2$ catalysts arises from increased molecular strain and/or rehybridization during adsorption over single Pd atoms. However, it seems likely that the higher electron density of single Pd atoms within the alloy surface would favor charge transfer into the π^* molecular orbitals of acetylene and consequent destabilization of the reactant triple bond. The difference in apparent activation energies may also reflect the ease of C_2H_4 desorption, because the alloyed Pd single-atom catalyst exhibits lower C_2H_4 initial adsorption enthalpies relative to its monometallic Pd counterpart,[31] which in turn would account for the higher ethylene selectivity of the bimetallic alloy system.

4. CONCLUSIONS

Ag alloyed Pd single-atom catalysts prepared over a silica gel support by simple incipient wetness coimpregnation employing only ppm levels of Pd exhibit excellent catalytic performance for the selective hydrogenation of acetylene under simulated front-end conditions. High-temperature prereduction promotes sintering of bimetallic nanoparticles, accompanied by silver surface segregation and charge transfer from Ag to Pd, resulting in an optimal Pd/Ag surface composition and surface ensembles possessing isolated electron-rich Pd atoms. The combination of the preceding geometric and electronic interactions between Ag and Pd renders the resulting Ag alloyed Pd single-atom catalysts as exceptional for the selective hydrogenation of acetylene in an ethylene-rich stream, a consequence of facile acetylene activation and weak adsorption of the resulting reactively formed ethylene product.

■ ASSOCIATED CONTENT

Supporting Information

The Supporting Information is available free of charge on the ACS Publications website at DOI: 10.1021/acscatal.5b00700.

Catalytic performance of Ag/SiO_2 and $Pd_{0.01}/SiO_2$ materials, HAADF-STEM results for calcined Ag/SiO_2 and $AgPd_{0.025}/SiO_2$, TPR and surface elemental analysis (PDF)

■ AUTHOR INFORMATION

Corresponding Authors

*E-mail: aqwang@dicp.ac.cn.
*E-mail: taozhang@dicp.ac.cn.

DOI: 10.1021/acscatal.5b00700
ACS Catal. 2015, 5, 3717−3725

Author Contributions

[#]These authors contributed equally to this work (G.X.P. and X.Y.L.).

Notes

The authors declare no competing financial interest.

■ ACKNOWLEDGMENTS

The authors are grateful to the National Science Foundation of China (21176235, 21173218, 21303194, 21373206, and 21476227), the Hundred Talents Program of Dalian Institute of Chemical Physics, the Key Research Programme of the Chinese Academy of Science (Grant No. KGZD-EW-T05), the EPSRC (EP/G007594/3) for financial support and a Leadership Fellowship (AFL) and the Royal Society for the award of an Industry Fellowship (KW). The authors also thank the BL14W at the SSRF for the XAS experiment.

■ REFERENCES

(1) McGown, W. T.; Kemball, C.; Whan, D. A.; Scurrell, M. S. *J. Chem. Soc., Faraday Trans. 1* **1977**, *73*, 632−647.
(2) Huang, W.; McCormick, J. R.; Lobo, R. F.; Chen, J. G. *J. Catal.* **2007**, *246*, 40−51.
(3) Rahimpour, M. R.; Dehghani, O.; Gholipour, M. R.; Shokrollahi Yancheshmeh, M. S.; Seifzadeh Haghighi, S.; Shariati, A. *Chem. Eng. J.* **2012**, *198*−*199*, 491−502.
(4) Mei, D.; Neurock, M.; Smith, C. M. *J. Catal.* **2009**, *268*, 181−195.
(5) Shi, C.; Hoisington, R.; Jang, B. W.-L. *Ind. Eng. Chem. Res.* **2007**, *46*, 4390−4395.
(6) Borodziński, A.; Bond, G. C. *Catal. Rev.: Sci. Eng.* **2008**, *50*, 379−469.
(7) Kim, S. K.; Kim, C.; Lee, J. H.; Kim, J.; Lee, H.; Moon, S. H. *J. Catal.* **2013**, *306*, 146−154.
(8) Benavidez, A. D.; Burton, P. D.; Nogales, J. L.; Jenkins, A. R.; Ivanov, S. A.; Miller, J. T.; Karim, A. M.; Datye, A. K. *Appl. Catal., A* **2014**, *482*, 108−115.
(9) Yang, B.; Burch, R.; Hardacre, C.; Headdock, G.; Hu, P. *J. Catal.* **2013**, *305*, 264−276.
(10) Ahn, I. Y.; Lee, J. H.; Kim, S. K.; Moon, S. H. *Appl. Catal., A* **2009**, *360*, 38−42.
(11) Sárkány, A.; Weiss, A. H.; Guczi, L. *J. Catal.* **1986**, *98*, 550−553.
(12) Crespo-Quesada, M.; Yarulin, A.; Jin, M.; Xia, Y.; Kiwi-Minsker, L. *J. Am. Chem. Soc.* **2011**, *133*, 12787−12794.
(13) Sárkány, A.; Geszti, O.; Sáfrán, G. *Appl. Catal., A* **2008**, *350*, 157−163.
(14) Lee, J. H.; Kim, S. K.; Ahn, I. Y.; Kim, W.-J.; Moon, S. H. *Catal. Commun.* **2011**, *12*, 1251−1254.
(15) Han, Y.; Peng, D.; Xu, Z.; Wan, H.; Zheng, S.; Zhu, D. *Chem. Commun.* **2013**, *49*, 8350−8352.
(16) Kim, S. K.; Lee, J. H.; Ahn, I. Y.; Kim, W.-J.; Moon, S. H. *Appl. Catal., A* **2011**, *401*, 12−19.
(17) Kim, E.; Shin, E. W.; Bark, C. W.; Chang, I.; Yoon, W. J.; Kim, W.-J. *Appl. Catal., A* **2014**, *471*, 80−83.
(18) Kang, J. H.; Shin, E. W.; Kim, W. J.; Park, J. D.; Moon, S. H. *J. Catal.* **2002**, *208*, 310−320.
(19) Kim, W.-J.; Ahn, I. Y.; Lee, J.-H.; Moon, S. H. *Catal. Commun.* **2012**, *24*, 52−55.
(20) Teschner, D.; Borsodi, J.; Wootsch, A.; Revay, Z.; Havecker, M.; Knop-Gericke, A.; Jackson, S. D.; Schlogl, R. *Science* **2008**, *320*, 86−9.
(21) Qiao, B. T.; Wang, A. Q.; Yang, X. F.; Allard, L. F.; Jiang, Z.; Cui, Y. T.; Liu, J. Y.; Li, J.; Zhang, T. *Nat. Chem.* **2011**, *3*, 634−641.
(22) Lin, J.; Wang, A. Q.; Qiao, B. T.; Liu, X. Y.; Yang, X. F.; Wang, X. D.; Liang, J.; Li, J.; Liu, J. Y.; Zhang, T. *J. Am. Chem. Soc.* **2013**, *135*, 15314−15317.
(23) Wei, H. S.; Liu, X. Y.; Wang, A. Q.; Zhang, L. L.; Qiao, B. T.; Yang, X. F.; Huang, Y. Q.; Miao, S.; Liu, J. Y.; Zhang, T. *Nat. Commun.* **2014**, *5*, 5634.
(24) Sun, S.; Zhang, G.; Gauquelin, N.; Chen, N.; Zhou, J.; Yang, S.; Chen, W.; Meng, X.; Geng, D.; Banis, M. N.; et al. *Sci. Rep.* **2013**, *3*, Article no. 1775.
(25) Yang, M.; Li, S.; Wang, Y.; Herron, J. A.; Xu, Y.; Allard, L. F.; Lee, S.; Huang, J.; Mavrikakis, M.; Flytzani-Stephanopoulos, M. *Science* **2014**, *346*, 1498−1501.
(26) Yang, X.-F.; Wang, A.-Q.; Qiao, B.-T.; Li, J.; Liu, J.-Y.; Zhang, T. *Acc. Chem. Res.* **2013**, *46*, 1740−1748.
(27) Zhang, L.; Wang, A.; Miller, J. T.; Liu, X.; Yang, X.; Wang, W.; Li, L.; Huang, Y.; Mou, C.-Y.; Zhang, T. *ACS Catal.* **2014**, *4*, 1546−1553.
(28) Zhang, H. J.; Watanabe, T.; Okumura, M.; Haruta, M.; Toshima, N. *Nat. Mater.* **2012**, *11*, 49−52.
(29) Boucher, M. B.; Zugic, B.; Cladaras, G.; Kammert, J.; Marcinkowski, M. D.; Lawton, T. J.; Sykes, E. C. H.; Flytzani-Stephanopoulos, M. *Phys. Chem. Chem. Phys.* **2013**, *15*, 12187−12196.
(30) Kyriakou, G.; Boucher, M. B.; Jewell, A. D.; Lewis, E. A.; Lawton, T. J.; Baber, A. E.; Tierney, H. L.; Sykes, E. C. H.; Flytzani-Stephanopoulos, M. *Science* **2012**, *335*, 1209−1212.
(31) Pei, G. X.; Liu, X. Y.; Wang, A.; Li, L.; Huang, Y.; Zhang, T.; Lee, J. W.; Jang, B. W. L.; Mou, C.-Y. *New J. Chem.* **2014**, *38*, 2043−2051.
(32) Lee, A. F.; Ellis, C. V.; Wilson, K.; Hondow, N. S. *Catal. Today* **2010**, *157*, 243−249.
(33) Li, L.; Wang, X. D.; Shen, J. Y.; Zhou, L. X.; Zhang, T. *Chin. J. Catal.* **2003**, *24*, 872−876.
(34) Liu, X.; Mou, C.-Y.; Lee, S.; Li, Y.; Secrest, J.; Jang, B. W. L. *J. Catal.* **2012**, *285*, 152−159.
(35) Liu, X.; Li, Y.; Lee, J. W.; Hong, C.-Y.; Mou, C.-Y.; Jang, B. W. L. *Appl. Catal., A* **2012**, *439*−*440*, 8−14.
(36) Lee, J. W.; Liu, X.; Mou, C.-Y. *J. Chin. Chem. Soc.* **2013**, *60*, 907−914.
(37) Liu, X.; Wang, A.; Yang, X.; Zhang, T.; Mou, C.-Y.; Su, D.-S.; Li, J. *Chem. Mater.* **2009**, *21*, 410−418.
(38) Slanac, D. A.; Hardin, W. G.; Johnston, K. P.; Stevenson, K. J. *J. Am. Chem. Soc.* **2012**, *134*, 9812−9819.
(39) Qu, Z.; Huang, W.; Cheng, M.; Bao, X. *J. Phys. Chem. B* **2005**, *109*, 15842−15848.
(40) Qu, Z.; Ke, G.; Wang, Y.; Liu, M.; Jiang, T.; Gao, J. *Appl. Surf. Sci.* **2013**, *277*, 293−301.
(41) Wang, A.-Q.; Liu, J.-H.; Lin, S. D.; Lin, T.-S.; Mou, C.-Y. *J. Catal.* **2005**, *233*, 186−197.
(42) Huang, D. C.; Chang, K. H.; Pong, W. F.; Tseng, P. K.; Hung, K. J.; Huang, W. F. *Catal. Lett.* **1998**, *53*, 155−159.
(43) Lamb, R. N.; Ngamsoma, B.; Trimmc, D. L.; Gong, B.; Silveston, P. L.; Praserthdam, P. *Appl. Catal., A* **2004**, *268*, 43−50.
(44) Wei, X.; Yang, X.-F.; Wang, A.-Q.; Li, L.; Liu, X.-Y.; Zhang, T.; Mou, C.-Y.; Li, J. *J. Phys. Chem. C* **2012**, *116*, 6222−6232.
(45) McCue, A. J.; McRitchie, C. J.; Shepherd, A. M.; Anderson, J. A. *J. Catal.* **2014**, *319*, 127−135.
(46) Zhu, B.; Thrimurthulu, Gode.; Delannoy, L.; Louis, C.; Mottet, C.; Creuze, J.; Legrand, B.; Guesmi, H. *J. Catal.* **2013**, *308*, 272−281.
(47) Skriver, H. L.; Rosengaard, N. M. *Phys. Rev. B: Condens. Matter Mater. Phys.* **1992**, *46*, 7157−7168.
(48) Li, M.; Shen, J. *Thermochim. Acta* **2001**, *379*, 45−50.
(49) Sheth, P. A.; Neurock, M.; Smith, C. M. *J. Phys. Chem. B* **2005**, *109*, 12449−12466.
(50) Zhang, Y.; Diao, W.; Williams, C. T.; Monnier, J. R. *Appl. Catal., A* **2014**, *469*, 419−426.
(51) Molero, H.; Stacchiola, D.; Tysoe, W. T. *Catal. Lett.* **2005**, *101*, 145−149.
(52) González, S.; Neyman, K. M.; Shaikhutdinov, S.; Freund, H.-J.; Illas, F. *J. Phys. Chem. C* **2007**, *111*, 6852−6856.

DOI: 10.1021/acscatal.5b00700
ACS Catal. 2015, 5, 3717−3725